A multivariate WCAWE for parametric model order reduction

R. Rumpler [1,2], **Q. Aumann** [3]
[1] KTH Royal Institute of Technology, MWL Laboratory for Sound and Vibration Research,
Teknikringen 8, SE-100 44 Stockholm, Sweden
e-mail: **rumpler@kth.se**

[2] KTH Royal Institute of Technology, The Centre for ECO2 Vehicle Design,
Teknikringen 8, SE-100 44 Stockholm, Sweden

[3] Max Planck Institute for Dynamics of Complex Technical Systems,
Sandtorstraße 1, 39106 Magdeburg, Germany

Abstract
Engineering applications often depend on multiple parameters, leading to a need for increasingly complex problems to be solved by numerical methods. The use of so-called parametric reduced-order models, based on the underlying physics, has proved to be an efficient approach to address a prohibitive computational cost with increasing dimensionality of the parametric space, while offering the prospect of an accurate approximation of the original problem. In this contribution, a multivariate version of the well-conditioned asymptotic waveform evaluation (WCAWE) algorithm is presented, namely the MWCAWE, in order to extend its applicability to parametric problems. It is applied in an adaptive algorithm based on a residue-based contour following approach. This algorithm computes reduced-order models of bi-variate acoustic problems where frequency and a material parameter are considered. A poro-acoustic application is presented, highlighting the potential of the multi-interval strategy for parametric applications.

1 Introduction

Engineering applications, such as optimisation, design and control problems, often require multiple, fast evaluations of solutions associated with numerical models depending on multiple parameters, such as the driving frequency or material properties. These may be efficiently performed with the introduction of surrogate models approximating the input-output behaviour of the original system while retaining the dependency on certain model parameters. For this purpose, a wide range of parametric model order reduction (pMOR) approaches have been proposed and investigated in the recent years [1]. Among these, projection-based methods occupy a central place, essentially consisting of global and local approaches. While local pMOR methods focus on multiple local reduction matrices to be interpolated in order to determine a new reduced-order model [2, 3, 4], global pMOR approaches generally perform recombination of projection matrices to generate a single representative projection matrix [5, 6, 7].

In this paper, we present the Multivariate Well-Conditioned Asymptotic Waveform Evaluation (MWCAWE). It is a projection-based global pMOR approach extending the established Well-Conditioned Asymptotic Waveform Evaluation (WCAWE) method [8, 9], which has proved to be an efficient approach for frequency sweep problems [10, 11]. WCAWE ensures rational interpolation up to an arbitrary order at certain expansion points in the frequency domain. The gist of extending WCAWE to MWCAWE is to also consider derivatives of the system regarding the other parameters which should be retained in the reduced space, here for instance a material parameter. The MWCAWE basis computation involves combinations of derivatives regarding the involved parameters at each expansion point in the considered parameter space. It follows a recombination

and truncation step which ensures an appropriate size of the reduction bases corresponding to each expansion point. Multiple local bases are combined in the global pMOR approach both to increase the accuracy locally and for the complete parameter space. Although a global pMOR method may lead to larger reduced-order models, accuracy of the approximation and computational cost associated with the projection basis generation may justify the choice of a global method over a local approach.

The rest of the article is structured as follows: In section 2, the MWCAWE approach is presented, after a summary of the original WCAWE algorithm. The proposed algorithm for a multi-interval strategy is proposed in section 3, including a residue-based error estimator and a contour-following approach for the bivariate case. A poro-acoustic application is then presented in section 4, showing the ability of the MWCAWE approach to provide a good approximation over the entire parametric domain of interest.

2 Introducing the MWCAWE

2.1 The univariate WCAWE

The starting point of the WCAWE-based parametric sweep is given by a linear system,

$$\mathbf{Z}(\mathbf{x})\mathbf{u}(\mathbf{x}) = \mathbf{f}(\mathbf{x}), \tag{1}$$

where $\mathbf{x}$ may be a vector of N_x independent variables corresponding to the parametric problem of interest including, e.g. the angular frequency ω, material parameters, etc. For the original univariate case discussed in [8], this vector reduces to a scalar such that $\mathbf{x} = x_1$. In a finite element (FE) problem, $\mathbf{Z}(\mathbf{x}) \in \mathbb{C}^{\mathrm{N}_n \times \mathrm{N}_n}$ represents the system matrix of the discretised problem and $\mathbf{u}(\mathbf{x}), \mathbf{f}(\mathbf{x}) \in \mathbb{C}^{\mathrm{N}_n}$ the solution vector and the vector of externally applied loads, respectively.

As N_n is typically large, the computational cost of solving eq. (1) can be reduced by finding a system

$$\mathbf{Z}_{\mathbf{s}_n}(\mathbf{x})\boldsymbol{\alpha}_{\mathbf{s}_n}(\mathbf{x}) = \mathbf{f}_{\mathbf{s}_n}(\mathbf{x}), \tag{2}$$

of much smaller dimension $\mathrm{N_V}$ whose solution vector approximates the solution to the original system in a subspace spanned by a matrix $\mathbf{V} \in \mathbb{C}^{\mathrm{N}_n \times \mathrm{N_V}}$, such that

$$\mathbf{u}(\mathbf{x}) \approx \hat{\mathbf{u}}_{\mathbf{s}_n}(\mathbf{x}) = \mathbf{V}\boldsymbol{\alpha}_{\mathbf{s}_n}(\mathbf{x}). \tag{3}$$

This projection-based approach, allowing the solution of a reduced set of equations in order to obtain an approximation for eq. (1), relies on the efficient construction of the reduction matrix $\mathbf{V}_{\mathbf{s}_n}$. A proper choice of $\mathbf{V}_{\mathbf{s}_n}$ emerges from successive derivatives of the solution vector in eq. (1) at a specific point in the parameter space $\mathbf{x} = \mathbf{s}_n$, $\mathbf{s}_n = (x_{1n}, \cdots, x_{\mathrm{N}_x n})$ being further referred to as the n-indexed reference point of $\mathbf{V}_{\mathbf{s}_n}$. For the original univariate case, i.e. associated with the WCAWE algorithm, $\mathrm{N}_x = 1$ and this reference point reduces to the scalar $\mathbf{s}_n = x_{1n}$. The WCAWE algorithm [9, 8] provides a robust generation of this sequence of successive derivatives, overcoming the inherent ill-conditioning of the direct approach which is, e.g., used in the computation of the component-wise Padé approximants [12, 13, 11] and in the generation of Nested Padé approximants [14, 15]. The resulting well-conditioned reduction matrix $\mathbf{V}_{\mathbf{s}_n}$, consisting of $\mathrm{N_V}$ orthonormalised basis vectors, allows for a robust, non-stagnating convergence upon increasing the size of the subspace spanned and ensures eq. (3) in the vicinity of $\mathbf{x} = \mathbf{s}_n$. This projection

$$\mathbf{V}_{\mathbf{s}_n}^{\mathsf{H}}\mathbf{Z}(\mathbf{x})\mathbf{V}_{\mathbf{s}_n}\boldsymbol{\alpha}_{\mathbf{s}_n}(\mathbf{x}) = \mathbf{V}_{\mathbf{s}_n}^{\mathsf{H}}\mathbf{f}(\mathbf{x}), \tag{4}$$

with $\mathbf{Z}_{\mathbf{s}_n}(\mathbf{x}) = \mathbf{V}_{\mathbf{s}_n}^{\mathsf{H}}\mathbf{Z}(\mathbf{x})\mathbf{V}_{\mathbf{s}_n}$ and $\mathbf{f}_{\mathbf{s}_n}(\mathbf{x}) = \mathbf{V}_{\mathbf{s}_n}^{\mathsf{H}}\mathbf{f}(\mathbf{x})$ leads to the reduced system eq. (2). The superscript $(\cdot)^{\mathsf{H}}$ denotes a Hermite transpose. In the context of an FE solution, eq. (4) is advantageously solved if the system matrix involved in the transformation, $\mathbf{Z}(\mathbf{x})$, is not reevaluated after an assembly procedure for each set of parametric vectors $\mathbf{x}$, but rather broken down in a linear combination of $\mathbf{x}$-independent global matrices.

2.2 The multivariate MWCAWE

A generic expression of the multivariate WCAWE algorithm (referred to as the MWCAWE in the following), as proposed in this contribution, may be given in $\mathbf{x} = \mathbf{s}_n$ by the following recursive, multiple right-hand-side (RHS) procedure adapted from the univariate case in [9, 8, 16],

$$\begin{cases} \mathbf{Z}^{(0)}\overline{\mathbf{v}}_1 = \mathbf{F}^{(0)} \\ \qquad Normalisation \;\; \overline{\mathbf{v}}_1 \longrightarrow \mathbf{v}_1 \\ \mathbf{Z}^{(0)}\overline{\mathbf{v}}_2 = \mathbf{F}^{(1)}\mathbf{e}_1^{\mathsf{T}}\mathbf{P}_{\mathbf{Q_1}}(2,1)\mathbf{e}_1 - \mathbf{Z}^{(1)}\mathbf{v}_1 \\ \qquad \text{Orthonormalisation} \;\; \overline{\mathbf{v}}_2 \longrightarrow \mathbf{v}_2 \\ \qquad \vdots \\ \mathbf{Z}^{(0)}\overline{\mathbf{v}}_n = \left(\sum_{j=1}^{(n-1)} \left(\mathbf{F}^{(n)}\mathbf{e}_1^{\mathsf{T}}\mathbf{P}_{\mathbf{Q_1}}(n,j)\mathbf{e}_{n-j} \right) - \mathbf{Z}^{(1)}\mathbf{v}_{n-1} \right. \\ \qquad\qquad \left. - \sum_{j=2}^{(n-1)} \left(\mathbf{Z}^{(j)}\mathbf{v}_{n-j}\mathbf{P}_{\mathbf{Q_2}}(n,j)\mathbf{e}_{n-j} \right) \right) \\ \qquad \text{Orthonormalisation} \;\; \overline{\mathbf{v}}_n \longrightarrow \mathbf{v}_n \\ \qquad \vdots \\ \mathbf{Z}^{(0)}\overline{\mathbf{v}}_{\mathrm{N_V}} = \left(\sum_{j=1}^{(\mathrm{N_V}-1)} \left(\mathbf{F}^{(\mathrm{N_V})}\mathbf{e}_1^{\mathsf{T}}\mathbf{P}_{\mathbf{Q_1}}(\mathrm{N_V},j)\mathbf{e}_{\mathrm{N_V}-j} \right) - \mathbf{Z}^{(1)}\mathbf{v}_{\mathrm{N_V}-1} \right. \\ \qquad\qquad \left. - \sum_{j=2}^{(\mathrm{N_V}-1)} \left(\mathbf{Z}^{(j)}\mathbf{v}_{\mathrm{N_V}-j}\mathbf{P}_{\mathbf{Q_2}}(\mathrm{N_V},j)\mathbf{e}_{\mathrm{N_V}-j} \right) \right) \\ \qquad \text{Orthonormalisation} \;\; \overline{\mathbf{v}}_{\mathrm{N_V}} \longrightarrow \mathbf{v}_{\mathrm{N_V}} \end{cases} \tag{5}$$

where a modified Gram-Schmidt orthonormalisation step is performed between each vector generation by the multiple RHS systems in eq. (5), and where

- $\mathbf{Z}^{(k)}$ stands for the differentiation of the system matrix $\mathbf{Z}$ in $\mathbf{x} = \mathbf{s}_n$ to the "cumulative" multivariate order k, regardless of the distribution of these partial derivatives between the independent variables x_j, $j = 1, \ldots, \mathrm{N}_x$. In other words, given the notation $\partial_{x_j}^{i_j}(\cdot)$ for the partial derivative with respect to x_j at order i_j, and the convention $\partial_{x_j}^{0}(\cdot) = (\cdot)$, then $\mathbf{Z}^{(k)}$ results from the summed partial derivative orders such that
$$\mathbf{Z}^{\left(\sum_{j=1}^{\mathrm{N}_x} i_j\right)} = \left(\prod_{j=1}^{\mathrm{N}_x} \partial_{x_j}^{i_j} \right) \mathbf{Z}, \tag{6}$$
with the aforementioned convention implying that $\mathbf{Z}^{(0)} = \mathbf{Z}$ (dependency on $\mathbf{x}$ omitted).
- $\mathbf{e}_k$ is a unitary standard basis vector associated with the k^{th} component of the solution vector,
- $\overline{\mathbf{v}}_k$ is the non-orthonormalised vector generated in the k^{th} iteration of the procedure,
- $\mathbf{v}_k$ is the basis vector orthonormalised against $\mathbf{v}_{k-1}$, generated after the k^{th} iteration of the procedure,
- $\mathbf{P}_{\mathbf{Q}_\omega}(\alpha, \beta)$, $\omega = 1, 2$, corresponds to the RHS correction terms, chosen to be associated with the modified Gram-Schmidt orthonormalisation process [8].

The resulting orthonormalised and non-orthonormalised bases, $\mathbf{V}_{\mathbf{s}_n} = [\mathbf{v}_1 \cdots \mathbf{v}_{\mathrm{N_V}}]$ and $\overline{\mathbf{V}}_{\mathbf{s}_n} = [\overline{\mathbf{v}}_1 \cdots \overline{\mathbf{v}}_{\mathrm{N_V}}]$ respectively, are related by

$$\mathbf{V}_{\mathbf{s}_n} = \overline{\mathbf{V}}_{\mathbf{s}_n}\mathbf{Q}^{-1}, \tag{7}$$

where $\mathbf{Q}$ is an $\mathrm{N_V} \times \mathrm{N_V}$ upper triangular, non-singular matrix containing the modified Gram-Schmidt coefficients. More precisely, column k of $\mathbf{Q}$ contains the successive coefficients resulting from the projection

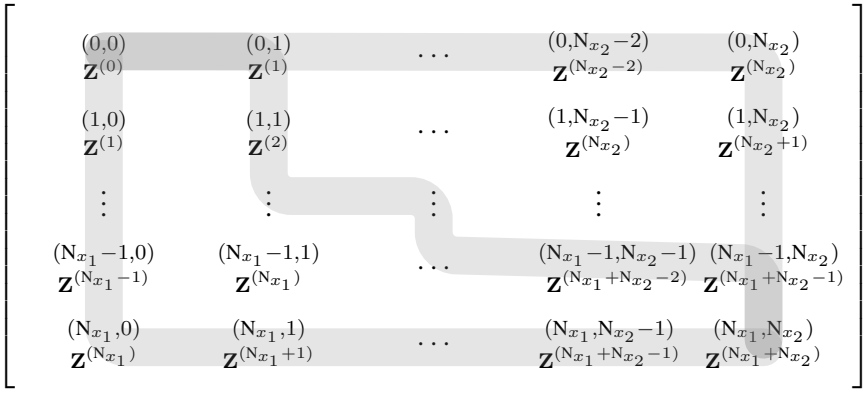

Figure 1: Illustration of three possible bivariate derivation paths for the system matrix $\mathbf{Z}$ up to the "cumulated" order of partial derivatives $(\mathrm{N}_{x_1} + \mathrm{N}_{x_2})$.

of the partially orthonormalised $\overline{\mathbf{v}}_k$ on the orthnormalised vectors $\mathbf{v}_j$, $j < k$, and Q_{kk} corresponds to the norm of $\mathbf{v}_k$ before its normalisation. The correction terms $\mathbf{P}_{\mathbf{Q}_\omega}(\alpha, \beta)$, $\omega = 1, 2$, are given by the following product of block matrices extracted from $\mathbf{Q}$,

$$\mathbf{P}_{\mathbf{Q}_\omega}(\alpha, \beta) = \prod_{t=\omega}^{\beta} \mathbf{Q}^{-1}_{[t:\alpha-\beta+t-1, t:\alpha-\beta+t-1]}. \tag{8}$$

Further discussions on the choice of the RHS correction coefficients other than associated with the Gram-Schmidt coefficients, may be found in [8]. The approximated solution may be evaluated at all degrees of freedom (DOFs) from the generalised coordinates vector $\boldsymbol{\alpha}_{\mathbf{s}_n}(\mathbf{x})$ following eq. (3).

Adapting the WCAWE algorithm from univariate to multivariate problems involves the generation of sequences of RHS vectors emerging from sequences of iteratively differentiated matrices $\mathbf{Z}^{(k)}$. The choice adopted here is to generate such sequences independently, thus generating a set of N_Σ bases $\left\{\mathbf{V}^1_{\mathbf{s}_n}, \cdots, \mathbf{V}^{\mathrm{N}_\Sigma}_{\mathbf{s}_n}\right\}$ associated with N_Σ sequences of iteratively differentiated matrices $\mathbf{Z}^{(k)}$. $\mathbf{Z}^{(k)}$, $k = 0,\ ...\ \mathrm{N_V} - 1$, represents the differentiated system matrix to a "cumulated" multivariate partial derivative order k, see the associated procedure of sequences of differentiation, for the bivariate case, illustrated in fig. 1. These bases, in principle all of the same size $\mathrm{N_V}$[1], each consist of orthonormalised basis vectors. However, these are naturally not mutually orthonormalised from one basis to the next. Additionally, it is not guaranteed that the N_Σ-sequences produce linearly independent subsets of vectors upon merging the resulting bases. A simple way to ensure this, as well as to reduce the basis to a minimum number of basis vectors, is to proceed with a compression, or a component selection, via a Singular Value Decomposition (SVD) of the merged set of bases [17, 18]. Either way, the initial step consists in an SVD of the merged basis after concatenation, $\mathbf{V}^{\text{mer}}_{\mathbf{s}_n} = \left[\mathbf{V}^1_{\mathbf{s}_n} \cdots \mathbf{V}^{\mathrm{N}_\Sigma}_{\mathbf{s}_n}\right]$, resulting in

$$\mathbf{V}^{\text{mer}}_{\mathbf{s}_n} = \sum_{i=1}^{\mathrm{N_{V^{mer}}}} \sigma_i \mathbf{w}^{\text{l}}_i \mathbf{w}^{\text{r}\mathsf{T}}_i, \tag{9}$$

where $\mathrm{N_{V^{mer}}} \leq \mathrm{N_V N_\Sigma}$ corresponds to the total number of basis vectors in $\mathbf{V}^{\text{mer}}_{\mathbf{s}_n}$ and σ_i, $\mathbf{w}^{\text{l}}_i$, and $\mathbf{w}^{\text{r}}_i$ correspond to the singular values and left and right singular vectors, respectively.

From the SVD, either the (left) singular vectors associated with the highest singular values are selected as the components of the final local reduction matrix, or the compression of the merged basis associated with the highest singular values is performed from the selected left singular vectors, right singular vectors and their corresponding singular values. Here the former approach is used, such that assuming a descending-ordered

[1] Strictly considered, the size of the bases in this N_Σ-sequence decreases by a dimensionality-dependent number of vectors for each basis added to the sequence, due to the partial overlap of consecutive sequences, see, e.g., fig. 1. This point is however marginally relevant here given the SVD step involved in the subsequent processing of these bases, see eqs. (9) and (10).

sequence of singular values $\left(\sigma_1 \cdots \sigma_{\mathrm{N_{V^{mer}}}}\right)$, the reduced, merged basis $\mathbf{V}^*_{\mathbf{s}_n}$ is

$$\mathbf{V}^*_{\mathbf{s}_n} = \left\{ \mathbf{w}^{\mathrm{l}}_i \mid i \in (1, \mathrm{N_{V^{mer}}}) \wedge \sigma_i \geq \sigma_{\mathrm{thresh}} \right\}, \tag{10}$$

where σ_{thresh} corresponds to the empirically chosen threshold value for the selection of the singular values resulting from the decomposition in eq. (9).

The resulting local projection basis $\mathbf{V}^*_{\mathbf{s}_n}$, consisting of $\mathrm{N_{V^*}}$ vectors, is then introduced in place of the generic, univariate transformation corresponding to eq. (3), such that

$$\hat{\mathbf{u}}^*_{\mathbf{s}_n}(\mathbf{x}) = \mathbf{V}^*_{\mathbf{s}_n}\, \boldsymbol{\alpha}^*_{\mathbf{s}_n}(\mathbf{x}), \tag{11}$$

leading to a reduced system associated with the initial problem in eq. (1), such that

$$\mathbf{V}^{*\,\mathsf{H}}_{\mathbf{s}_n} \mathbf{Z}(\mathbf{x}) \mathbf{V}^*_{\mathbf{s}_n} \boldsymbol{\alpha}^*_{\mathbf{s}_n}(\mathbf{x}) = \mathbf{V}^{*\,\mathsf{H}}_{\mathbf{s}_n} \mathbf{f}(\mathbf{x}), \tag{12}$$

involving $\mathrm{N_{V^*}} \leq \mathrm{N_{V^{mer}}}$ generalised coordinates in $\boldsymbol{\alpha}^*_{\mathbf{s}_n}(\mathbf{x})$.

3 A multi-interval approach: the bivariate case

In practice, a reduced-order model computed from a single reference point $\mathbf{s}_n$ may not be able to efficiently approximate the full-order model in the desired range of parameters. Introducing multiple expansion points $\mathbf{s}_n$ may increase the accuracy of the reduced-order model for wider parameter ranges, but each new expansion point requires the decomposition of the full order system matrix. Increasing the order of approximation is typically less computationally expensive, but the approximation quality may not significantly benefit from the higher orders and eventually stagnate. This implies a trade-off between increasing the order of approximation, reflected in the size of the basis $\mathrm{N_V}$ for a given reference point $\mathbf{s}_n$, and a multi-interval strategy involving several such reference points.

Regardless of the motivation for a multi-interval approximation, an assessment of the approximation error is a necessary prior step for an efficient, automated sampling of the parametric space, and discussed in the following section.

3.1 Error estimator

A residue-based error estimator is used to identify bounds of intervals of the approximated solution with a satisfying degree of accuracy. Such residual-based estimators have shown to be both efficient and accurate ways of tracking the approximation error [19, 20, 21, 22, 15, 23, 24, 25]. The residue-based error estimator approach implemented seeks to be relying on a unique set of local bases merged into $\mathbf{V}^*_{\mathbf{s}_n}$, see eq. (10), and a single evaluation of the error limited to a subset of necessary points in the parametric space. The residue is evaluated on the basis of the residual vector $\mathbf{r}^*_{\mathbf{s}_n}(\mathbf{x})$ associated with the approximated solution $\hat{\mathbf{u}}^*_{\mathbf{s}_n}(\mathbf{x})$, see eqs. (11) and (12), following a transformation with the merged local bases $\mathbf{V}^*_{\mathbf{s}_n}$ of eq. (10). This residual vector is given by

$$\mathbf{r}^*_{\mathbf{s}_n}(\mathbf{x}) = \mathbf{Z}(\mathbf{x})\, \hat{\mathbf{u}}^*_{\mathbf{s}_n}(\mathbf{x}) - \mathbf{f}(\mathbf{x}), \tag{13}$$

for a generic problem of the form of eq. (1). It may subsequently be used as an error indicator based on its ℓ^2 norm, such that,

$$\varepsilon^*_{\mathbf{s}_n}(\mathbf{x}) = \frac{||\mathbf{r}^*_{\mathbf{s}_n}(\mathbf{x})||_2}{\min\left(||\mathbf{r}^*_{\mathbf{s}_n}(\mathbf{x})||_2\right)}, \tag{14}$$

which is normalized with respect to the minimum residual norm evaluated, presumably corresponding to an $\mathbf{x}$ in the closest vicinity of $\mathbf{s}_n$, if an evaluation in $\mathbf{s}_n$ is excluded. This error estimator enables the search for bounds of convergence associated with each pair of basis and reference point, as further detailed in the next section.

3.2 Contour-following-based multi-interval strategy for the bivariate case

In order to establish a multi-interval strategy, i.e. defining a set of points $\{\mathbf{s}_1, \ldots, \mathbf{s}_n, \ldots, \mathbf{s}_\mathrm{N}\}$ at which local bases are to be calculated, the bounds of accuracy associated with each of these bases have to be estimated. This is here proposed to be done assuming a monotonic increase of the approximation error as the distance to the reference parametric point $\mathbf{s}_n$ increases, within the limit of relatively small approximation errors. A contour tracing algorithm is utilised, seeking to follow an error estimator isocontour corresponding to the predetermined tolerance ε_max, in order to approximate the required bounds. Starting from a point in parameter space close to $\mathbf{s}_1 = (x_{11}, x_{21})$, the algorithm seeks the first contour point, which is the first point in an arbitrarily chosen direction at which the approximation error is estimated to be larger than ε_max. It then iteratively determines the closed contour around the parameter region of sufficiently accurate approximation by a Moore-Neighbour approach. The estimation of such bounds of convergence subsequently allows to choose sequentially locations for new reference points $\mathbf{s}_n = (x_{1n}, x_{2n})$, $n = 2, \ldots, \mathrm{N}$, for the calculation of additional local bases. This opens the way for a multi-interval solution strategy, gradually filling the entire bivariate range of interest with sub-domains of satisfactory approximation, as described below.

Let Ω be a set of all vectors $\mathbf{x}_i$ where the solution to eq. (1) is sought to be approximated, and $\partial\Omega$ its outer boundary set. A sequential approach is considered in order to establish N local merged bases associated with a sequence of N reference points $\langle \mathbf{s}_n | \mathbf{s}_n \in \Omega \wedge n \in \{1, \mathrm{N}\} \rangle$. The algorithm aims at gradually filling the parametric domain of interest with converged sub-intervals. Each interval is bounded by a contour where the accuracy of the reduced-order model associated with the corresponding reference point is estimated to be sufficient. The number of local merged bases necessary to approximate the solution in the complete domain of interest Ω is iteratively determined given a tolerance for the error estimator ε_max, the bounds of the parametric space of interest $\partial\Omega$, as well as a gap-tolerance $\Delta_\mathrm{gap\_max}$, in terms of the maximum allowable distance between two neighbour domains of convergence. In this region none of the local merged bases $\mathbf{V}^*_{\mathbf{s}_n}$ fulfils the convergence criterion $\varepsilon^*_{\mathbf{s}_n}(\mathbf{x}) \leq \varepsilon_\mathrm{max}$. Since the introduction of a residual-based error estimator alleviates the need for multiple reduced-order models resulting from complementary approximations of the original model, the dimensions of the reduction bases are fixed a priori and set to be equal for all local bases.

Further, the set Ω_conv is introduced, comprising the parameter combinations for which at least one of the merged local bases fulfils the convergence criterion,

$$\Omega_\mathrm{conv} = \left\{ \mathbf{x} \mid \varepsilon^*_{\mathbf{s}_n}(\mathbf{x}) \leq \varepsilon_\mathrm{max} \wedge n \in \{1, \mathrm{N}\} \right\}. \tag{15}$$

$\partial\Omega_\mathrm{conv}$ is subsequently introduced as its boundary set, while its relative complement, where no local basis allows to reach an acceptable approximation, is denoted $\Omega_\mathrm{gap} = \Omega \setminus \Omega_\mathrm{conv}$. Additionally, associated with each of the reference points $\mathbf{s}_n$, the local merged basis denoted $\mathbf{V}^*_{\mathbf{s}_n}$ allows to approximate the solution for a subset $\Omega_{\mathbf{s}_n} \subseteq \Omega_\mathrm{conv}$. This local basis $\mathbf{V}^*_{\mathbf{s}_n}$ is obtained according to the details introduced in section 2.2, leading to eq. (10), whose procedure is referred to in Algorithm 1 as the function GETBASIS(). For each local basis, the isocontour associated with the error estimator tolerance ε_max is obtained according to the Moore-Neighbour contour tracing algorithm and referred to as the function GETCONTOUR(). The closure associated with the boundary set $\partial\Omega_{\mathbf{s}_n}$ is obtained via a function referred to as FILL(). Finally, the function D() refers to the signed distance function, returning the distance of a parameter combination $\mathbf{x}$ to a boundary $\partial\Omega$ or $\partial\Omega_\mathrm{conv}$, assuming here a convention of negative values inside Ω_conv and positive outside. A conceptual pseudocode of the multi-interval generation of these N local bases is presented in Algorithm 1.

Algorithm 1 leads to a set of N local bases $\mathbf{V}^*_{\mathbf{s}_n}$ associated with the reference points $\mathbf{s}_n$, $n = 1, \ldots, \mathrm{N}$. It is illustrated for a case consisting of four reference points in fig. 2. Depending on the choice of tolerance $\Delta_\mathrm{gap\_max}$, the domains of convergence associated with these local bases are not necessarily overlapping, which may lead to gaps in the domain where the approximation of the original solution is not fulfilling the sought degree of accuracy. It is, however, noteworthy that by construction, these bases are not expected to be consisting of vectors mutually linearly independent. According to the nature of the dependence of the response with respect to the set of variables in $\mathbf{x}$, neighbouring local bases may contribute to enriching the subspace spanned by each basis $\mathbf{V}^*_{\mathbf{s}_n}$, $n = 1, \ldots, \mathrm{N}$. These local bases may thus be advantageously recombined into a global basis, in particular in order to improve the accuracy of the approximation in the gaps, where no specific local basis is initially assigned. This recombination is in the following examples applied to form a single

Algorithm 1: Calculation of the multi-interval sub-bases

Result: A set of sub-bases with their estimated bounds of convergence

// Initialisation

$\varepsilon_{\text{max}} \leftarrow$ Max error tolerance

$\Delta_{\text{gap\_max}} \leftarrow$ Max allowable gap distance to any interval

Define Ω, $\partial\Omega$, $\Omega_{\text{conv}} = \emptyset$ // Domain and boundary sets

$\Omega_{\text{gap}} \leftarrow \Omega \setminus \Omega_{\text{conv}}$

// Starting basis from initial reference point $\mathbf{s}_1$

$\mathbf{s}_1 \leftarrow (x_{11}\ x_{21})$

$\mathbf{V}^*_{\mathbf{s}_1} \leftarrow$ GETBASIS($\mathbf{s}_1$,N_V,N_Σ)

$\partial\Omega_{\mathbf{s}_1} \leftarrow$ GETCONTOUR($\mathbf{s}_1$,$\mathbf{V}^*_{\mathbf{s}_1}$,$\varepsilon_{\text{max}}$)

$\Omega_{\mathbf{s}_1} \leftarrow$ FILL($\partial\Omega_{\mathbf{s}_1}$)

// Update convergence and gap sets

$\Omega_{\text{conv}} \leftarrow \Omega_{\text{conv}} \cup \Omega_{\mathbf{s}_1}$

$\Omega_{\text{gap}} \leftarrow \Omega \setminus \Omega_{\text{conv}}$

$Gap \leftarrow \text{MAX}\left\{\text{D}(\mathbf{x}, \partial\Omega_{\text{conv}} \cup \partial\Omega) \mid \mathbf{x} \in \Omega_{\text{gap}}\right\}$

$n \leftarrow 1$

// Calculation of subsequent sub-bases

while $Gap > \Delta_{\text{gap\_max}}$ **do**

  $n \leftarrow n + 1$

  $\mathbf{s}_n \leftarrow \text{ARGMAX}\left\{\text{D}(\mathbf{x}, \partial\Omega_{\text{conv}} \cup \partial\Omega) \mid \mathbf{x} \in \Omega_{\text{gap}}\right\}$

  $\mathbf{V}^*_{\mathbf{s}_n} \leftarrow$ GETBASIS($\mathbf{s}_n$,N_V,N_Σ)

  $\partial\Omega_{\mathbf{s}_n} \leftarrow$ GETCONTOUR($\mathbf{s}_n$,$\mathbf{V}^*_{\mathbf{s}_n}$,$\varepsilon_{\text{max}}$)

  $\Omega_{\mathbf{s}_n} \leftarrow$ FILL($\partial\Omega_{\mathbf{s}_n}$)

  // Update convergence and gap sets

  $\Omega_{\text{conv}} \leftarrow \Omega_{\text{conv}} \cup \Omega_{\mathbf{s}_n}$

  $\Omega_{\text{gap}} \leftarrow \Omega \setminus \Omega_{\text{conv}}$

  $Gap \leftarrow \text{MAX}\left\{\text{D}(\mathbf{x}, \partial\Omega_{\text{conv}} \cup \partial\Omega) \mid \mathbf{x} \in \Omega_{\text{gap}}\right\}$

end

global basis, which may, however, be easily adapted to only subsets of neighbouring local bases in cases of very large parametric domains. A natural way to recombine these is via an SVD, as already introduced for the sequences of local bases emerging from the partial differentiation process in section 2.2, implicitly performed in function GETBASIS() of Algorithm 1. Similarly to eq. (9), the merged basis matrix $\mathbf{V}^{*\text{mer}} = \left[\mathbf{V}^*_{\mathbf{s}_1} \cdots \mathbf{V}^*_{\mathbf{s}_\text{N}}\right]$ is decomposed following an SVD such that

$$\mathbf{V}^{*\text{mer}} = \sum_{i=1}^{\text{N}_{\text{V}^{*\text{mer}}}} \sigma_i^* \mathbf{w}_i^{\text{l}*} \mathbf{w}_i^{\text{r}*\text{T}}, \tag{16}$$

where $\text{N}_{\text{V}^{*\text{mer}}}$ corresponds to the total number of basis vectors in $\mathbf{V}^{*\text{mer}}$; σ_i^*, $\mathbf{w}_i^{\text{l}*}$, and $\mathbf{w}_i^{\text{r}*}$ correspond to the singular values and left and right singular vectors respectively. From the SVD, the left singular vectors associated with the highest singular values are selected as the components of the reduced merged basis $\mathbf{V}^{**}$, such that assuming a descending-ordered sequence of singular values $\left(\sigma_1^* \cdots \sigma^*_{\text{N}_{\text{V}^{*\text{mer}}}}\right)$, the reduced, merged basis is given by

$$\mathbf{V}^{**} = \left\{\mathbf{w}_i^{\text{l}*} \mid i \in (1, \text{N}_{\text{V}^{*\text{mer}}}) \wedge \sigma_i^* \geq \sigma_{\text{thresh}}\right\}, \tag{17}$$

where σ_{thresh} corresponds to an empirically chosen threshold value for the selection of the singular values resulting from the decomposition in eq. (16).

The resulting global reduction matrix $\mathbf{V}^{**}$, consisting of $\text{N}_{\text{V}^{**}}$ vectors, is then introduced in place of the

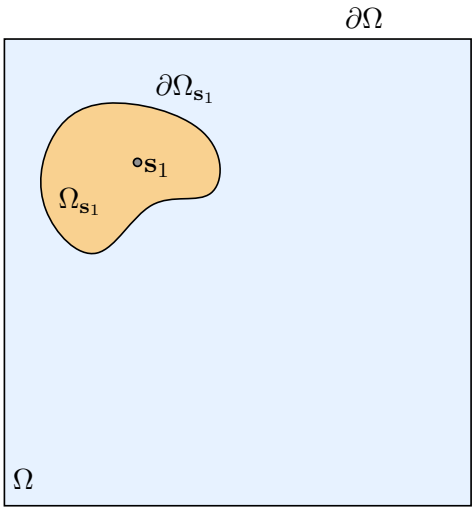

(a) Completed Moore-Neighbour algorithm for $\mathbf{s}_1$.

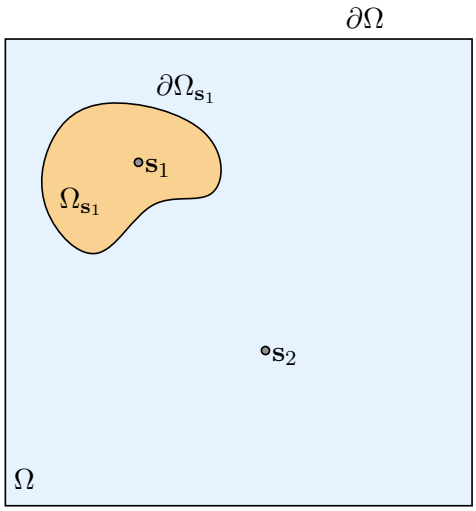

(b) New reference point $\mathbf{s}_2$ (cf. Algorithm 1, line 15).

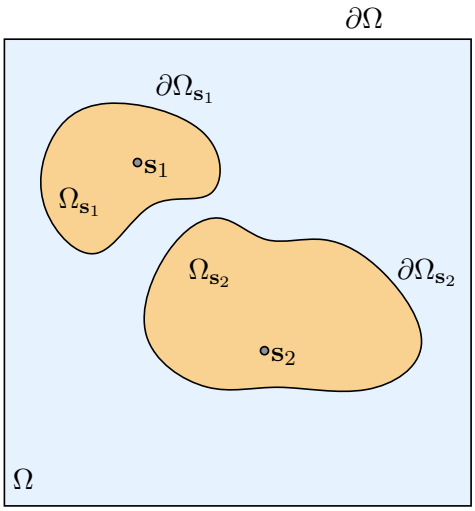

(c) Completed Moore-Neighbour algorithm for $\mathbf{s}_2$.

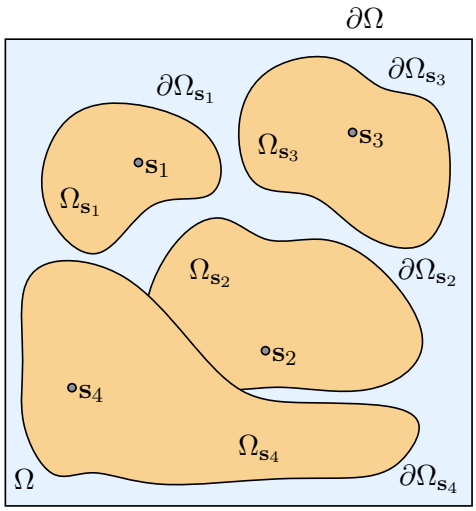

(d) After convergence.

Figure 2: Illustration of Algorithm 1. The domain of interest Ω is depicted in light blue, the converged contours $\Omega_{\mathbf{s}_n}$ in light orange.

single-interval transformation corresponding to eq. (11), such that,

$$\hat{\mathbf{u}}^{**}(\mathbf{x}) = \mathbf{V}^{**}\boldsymbol{\alpha}^{**}(\mathbf{x}). \tag{18}$$

This leads to a reduced system associated with the initial problem in eq. (1), such that,

$$\mathbf{V}^{**\mathsf{T}}\mathbf{Z}(\mathbf{x})\mathbf{V}^{**}\boldsymbol{\alpha}^{**}(\mathbf{x}) = \mathbf{V}^{**\mathsf{T}}\mathbf{f}(\mathbf{x}), \tag{19}$$

involving $\mathrm{N}_{\mathbf{V}^{**}} \leq \mathrm{N}_{\mathbf{V}^{*\mathrm{mer}}}$ generalised coordinates in $\boldsymbol{\alpha}^{**}(\mathbf{x})$.

4 Application

In order to evaluate the potential of the MWCAWE approach, it is here applied to a poro-acoustic test case.

4.1 Problem and reference solution

The MWCAWE approach and the associated sampling strategy is implemented for the approximation of a bivariate poro-acoustic problem, adapted from the model introduced in [26]. This problem models the interior cavity of a passenger train equipped with a $15\,\mathrm{cm}$ layer of sound absorbing porous material on the top surface. A time-harmonic point source is defined at a lower-back corner of the passenger cavity and parametric sweeps with respect to both the frequency and the static airflow resistivity of the porous layer are performed. All boundary walls are considered as rigid walls, except from the porous boundary. The discretised problem consists of around $\mathrm{N}_n \approx 300\,000$ DOFs. Assuming a poroelastic material where the motion of the skeleton may be neglected, the Delany-Bazley-Miki empirical model [27, 28] is used in order to describe the behaviour of the porous layer as an equivalent fluid. The acoustic response of the porous layer is thus governed by two independent variables: the frequency f and the static airflow resistivity Φ. The associated equivalent speed of sound $\tilde{c}_\mathrm{p}$ is complex-valued and frequency-dependent, and may be expressed as

$$\tilde{c}_\mathrm{p} = \sqrt{\frac{\widetilde{K}_\mathrm{eq}}{\widetilde{\rho}_\mathrm{eq}}}, \tag{20}$$

where the density $\widetilde{\rho}_\mathrm{eq}$ and bulk modulus $\widetilde{K}_\mathrm{eq}$ are complex-valued and frequency-dependent, given by

$$\widetilde{\rho}_\mathrm{eq}(f,\Phi) = \rho_0 \left[1 + \left(5.5 - 8.43i\right)\left(1000\frac{f}{\Phi}\right)^{-0.632}\right]\left[1 + \left(7.81 - 11.41i\right)\left(1000\frac{f}{\Phi}\right)^{-0.618}\right], \tag{21a}$$

$$\widetilde{K}_\mathrm{eq}(f,\Phi) = \rho_0 c_0^2 \frac{1 + \left(5.5 - 8.43i\right)\left(1000\frac{f}{\Phi}\right)^{-0.632}}{1 + \left(7.81 - 11.41i\right)\left(1000\frac{f}{\Phi}\right)^{-0.618}}, \tag{21b}$$

where $\tilde{(\cdot)}$ denotes a complex-valued quantity, i the imaginary unit, $\rho_0 = 1.21\,\mathrm{kg\,m^{-3}}$ is the ambient density of the air saturating the pores, and $c_0 = 343\,\mathrm{m\,s^{-1}}$ is the speed of sound in the air.

The discretised FE problem for two coupled domains governed by the Helmholtz equation (one with a fluid assumed to be inviscid, compressible, homogeneous, and the other with the equivalent fluid model for the fibrous material with high porosity aforementioned) may be presented in the following form

$$\left(\mathbf{K}_\mathrm{a} - \frac{\omega^2}{c_0^2}\mathbf{M}_\mathrm{a} + \mathbf{K}_\mathrm{p} - \frac{\omega^2}{\tilde{c}_\mathrm{p}^{\,2}}\mathbf{M}_\mathrm{p}\right)\mathbf{u} = \mathbf{f}, \tag{22}$$

where $(\cdot)_\mathrm{a}$ denote air cavity global matrices and $(\cdot)_\mathrm{p}$ porous global matrices. $\mathbf{u}$ is the vector of nodal unknowns (acoustic pressure fluctuation here). The right-hand-side vector $\mathbf{f}$, associated with the time-harmonic acoustic excitation is in practice only non-zero at a few DOFs. The FE problem in eq. (22) can again be expressed in the generic form of eq. (1)

$$\mathbf{Z}_\mathrm{pa}\left(f,\Phi\right)\mathbf{u}\left(f,\Phi\right) = \mathbf{f}, \tag{23}$$

and is thus suitable for the proposed multivariate approach.

Figure 3 illustrates the geometry of the cavity as well as the solution at a given point of the parametric sweep for a frequency of $f = 63\,\mathrm{Hz}$ and a flow resistivity of $\Phi = 25\,000\,\mathrm{N\,s\,m^{-4}}$. The reference solution for the bivariate parametric sweep, where $f \in [50, 150]\,\mathrm{Hz}$ and $\Phi \in [3000, 50000]\,\mathrm{N\,s\,m^{-4}}$, at a point in the lower-middle part of a cross-section at the front of the passenger cavity, is plotted in fig. 4. The solution is evaluated for a uniform distribution of frequency and flow resistivity in these ranges with increments of $1\,\mathrm{Hz}$ and $1000\,\mathrm{N\,s\,m^{-4}}$, respectively, leading to a grid of 4848 solution points to be evaluated for the domain of

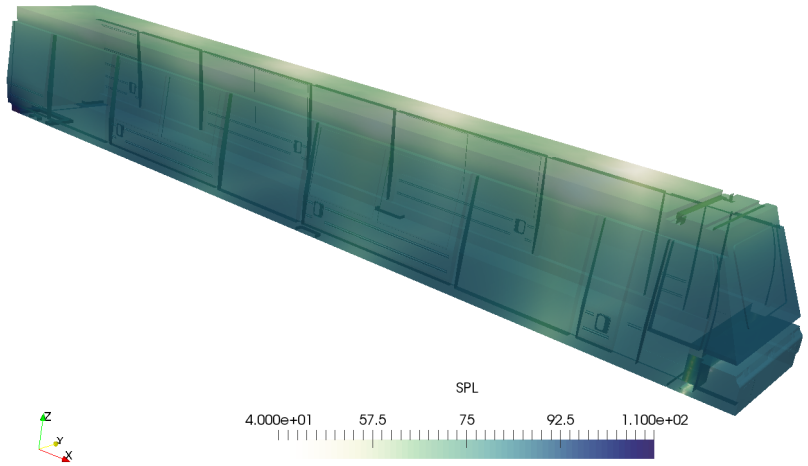

Figure 3: Sound pressure level of the damped solution at $f = 63\,\mathrm{Hz}$, $\Phi = 25\,000\,\mathrm{N\,s\,m^{-4}}$, scale $40 - 110\mathrm{dB}$.

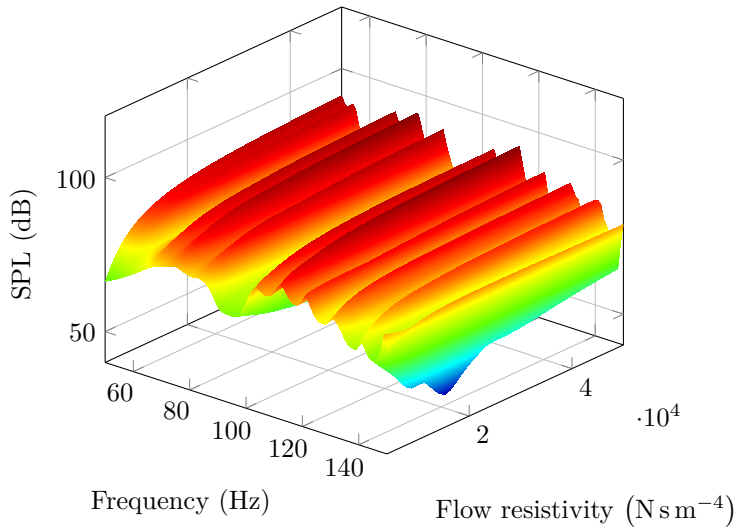

Figure 4: Reference solution. Sound pressure level at a point in the lower-middle part of a cross-section at the front of the passenger cavity, parametric solution, in dB.

interest. The non-damped cavity problem consists of 52 eigenfrequencies in the frequency ranged considered, see [26].

4.2 MWCAWE approximation

In order to illustrate the behaviour of the multi-point procedure introduced in section 2.2 combined with the associated residue-based contour-following approach, fixed orders of maximum partial derivatives are set a priori for all local bases. These are arbitrarily set to orders $\mathrm{N}_{x_1} = \mathrm{N_f} = 11$ for the frequency and $\mathrm{N}_{x_2} = \mathrm{N}_\Phi = 5$ for the flow resistivity, thus anticipating the fact that the solution is more sensitive to variations in frequency than flow resistivity in the bounds of interest. For a two-sequence approach, this leads to local merged bases consisting of $2\,(\mathrm{N_f} + \mathrm{N}_\Phi) = 32$ basis vectors, cf. section 2.2 and fig. 1. The starting reference point is chosen at $f = 88\,\mathrm{Hz}$ and $\Phi = 25\,000\,\mathrm{N\,s\,m^{-4}}$. For the contour following algorithm, the residual

error tolerance is set to $\varepsilon_{\max} = 1e7$, in practice involving a normalisation with respect to the residual error at the reference point for each interval. Finally, the gap tolerance for the iterative introduction of new reference points is set such that the maximum distance between two contours of convergence, $\Delta_{\text{gap\_max}}$, is of 10 units in the sense of the Chebyshev distance, or of 5 units for the distance between a contour and a boundary of the domain. These units correspond, for the considered bivariate problem, to the previously introduced uniform grid associated with frequency and flow resistivity increments. Thus, the domain of interest contains 4848 solution points.

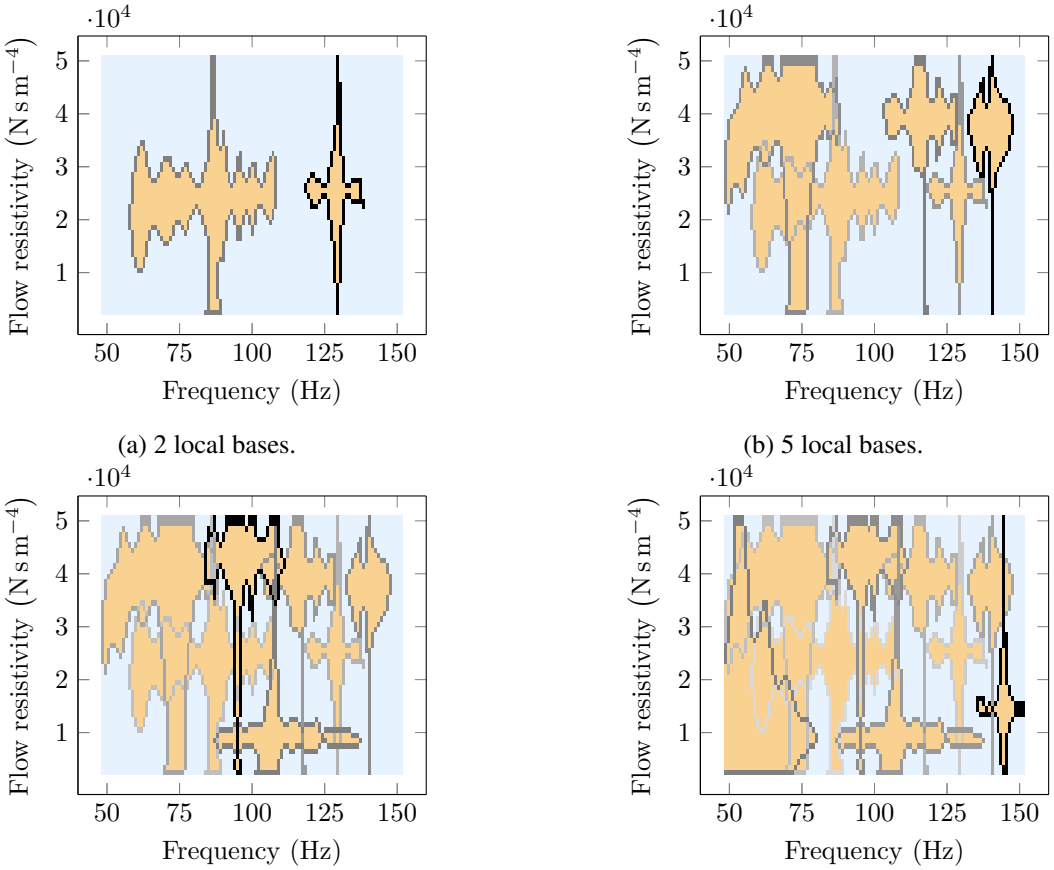

(a) 2 local bases.

(b) 5 local bases.

(c) 7 local bases.

(d) 9 local bases.

Figure 5: Contour-following, multi-interval calculation of local bases for the MWCAWE. Starting expansion point: $f = 88\,\text{Hz}$ and $\Phi = 25\,000\,\text{N s m}^{-4}$. Fixed partial derivative orders in frequency/flow resistivity: 11/5. Contours of convergence associated with the first 2, 5, 7, and 9 local bases. The regions with darker contours correspond to the latest calculated local bases.

Figure 5 shows 4 key steps associated with Algorithm 1. The sequence of fig. 5a to fig. 5d depicts an increasing number of convergence isocontours associated with local bases independently calculated from the reference points introduced at each iteration of Algorithm 1. The darker contours correspond to the latest addition in the successive iterations of the algorithm. Given the input parameters described above, the sequence ends after 9 local bases in fig. 5d. Note a few gaps remaining between the convergence contours, such as for low values of the flow resistivity in the ranges $[80, 88]$ Hz or $[112, 130]$ Hz. The gaps are in agreement with the introduced gap tolerance $\Delta_{\text{gap\_max}}$. These nine local bases are recombined into a single projection basis in an SVD step, see eq. (16). This recombination is further intended to improve the accuracy of the approximation in the gaps where all the neighbour local bases may contribute. In order both to ensure a well-conditioned reduced system of equations and to reduce the number of DOFs, the basis vectors associated with the lowest singular values are discarded, according to eq. (17), such that $\sigma_{\text{thresh}} = 1e{-}8 \cdot \sigma_{\max}$, where $\sigma_{\max}$ is the largest singular value. In the present case, this truncation results in downsizing the merged basis from $N_{V^{*\text{mer}}} = 288$ to $N_{V^{**}} = 275$ basis vectors. This minor reduction of the size of the basis shows the close-to-maximum dimension of the vector space spanned by the independently calculated and merged local bases.

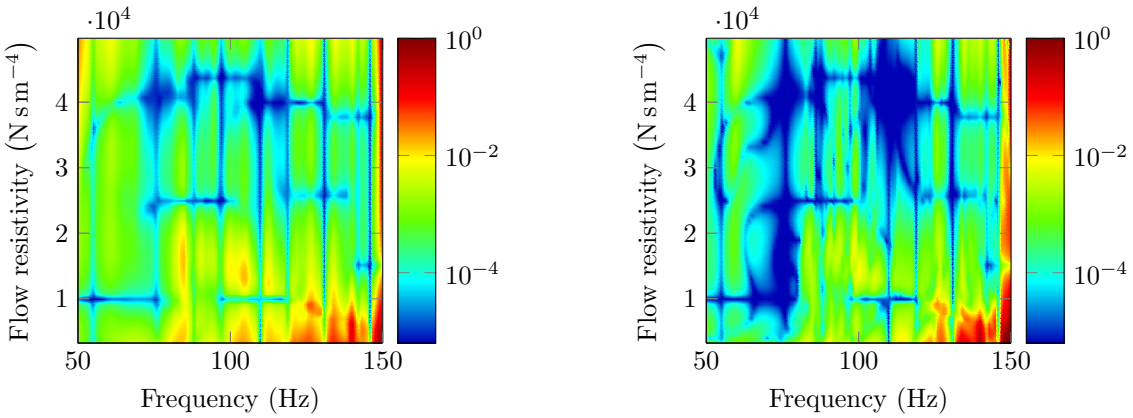

(a) Error estimation ε^*.

(b) Actual approximation error.

Figure 6: Error of the approximate solution from the merged bases associated with the contour of fig. 5. Fixed partial derivative orders in frequency/flow resistivity: 11/5, and 275 final basis vectors from 9 merged local bases.

In fig. 6 the resulting approximation error associated with the multi-point MWCAWE approach is plotted: the estimated error in fig. 6a and the actual difference to the reference solution in fig. 6b. A qualitative comparison between the plots shows the good correlation between the error estimator and the exact approximation error. Thus, the error estimator enables a fast evaluation of the bounds of convergence and the actual resulting approximation error associated with the MWCAWE. It is also noteworthy to mention that the error levels in the regions where gaps between the contours of convergence remained after all nine local bases are taken into consideration and merged into a single global reduced basis remain very low. The errors are mostly comparable to the levels within the bounds of convergence determined in fig. 5.

5 Conclusion

The MWCAWE, a multivariate model order reduction method relying on the WCAWE algorithm, is presented. It consists in a two-stage generation of local bases, subsequently recombined for a projection-based approach to approximate the full-order parametric model. At the heart of the method, a reduced set of partial derivation pathways of the parametric system matrices allow to generate local bases using the original WCAWE algorithm. The number of these partial derivation pathways is in principle linearly increasing with the parametric dimensionality. Additionally, in order to both limit the maximum partial derivative orders associated with a rapid increase of operations associated with the WCAWE algorithm and to improve the accuracy of the approximation in a given parametric domain, a sampling strategy is included. Here presented for the case of bivariate problems, it relies on a residue-based estimation of the approximation error combined with a contour-following algorithm, enabling to sequentially select new points outside the domain of convergence. The MWCAWE approach, combined with the multi-point strategy, is applied to a poro-acoustic light train cavity problem, and provides a good approximation over the entire parametric domain of interest with 9 recombined local bases. The associated residue-based estimator is shown to capture the main features of the approximation error. Specific ongoing perspectives to this contribution consist in adapting the contour-following approach to a compressed version allowing to efficiently adapt the multi-point strategy to higher dimensionalities.

References

[1] P. Benner, S. Gugercin, and K. Willcox, “A Survey of Projection-Based Model Reduction Methods for Parametric Dynamical Systems,” *SIAM Review*, vol. 57, no. 4, pp. 483–531, 2015.

[2] D. Amsallem and C. Farhat, "Interpolation Method for Adapting Reduced-Order Models and Application to Aeroelasticity," *AIAA Journal*, vol. 46, no. 7, pp. 1803–1813, 2008.

[3] J. Degroote, J. Vierendeels, and K. Willcox, "Interpolation among reduced-order matrices to obtain parameterized models for design, optimization and probabilistic analysis," *International Journal for Numerical Methods in Fluids*, vol. 63, no. 2, pp. 207–230, 2010.

[4] J. Borggaard, K. R. Pond, and L. Zietsman, "Parametric Reduced Order Models Using Adaptive Sampling and Interpolation," *IFAC Proceedings Volumes*, vol. 47, no. 3, pp. 7773–7778, 2014.

[5] L. Daniel, O. C. Siong, L. S. Chay, K. H. Lee, and J. White, "A Multiparameter Moment-Matching Model-Reduction Approach for Generating Geometrically Parameterized Interconnect Performance Models," *IEEE Transactions on Computer-Aided Design of Integrated Circuits and Systems*, vol. 23, no. 5, pp. 678–693, 2004.

[6] U. Baur, C. Beattie, P. Benner, and S. Gugercin, "Interpolatory Projection Methods for Parameterized Model Reduction," *SIAM Journal on Scientific Computing*, vol. 33, no. 5, pp. 2489–2518, 2011.

[7] P. Benner and L. Feng, "A Robust Algorithm for Parametric Model Order Reduction Based on Implicit Moment Matching," in *Reduced Order Methods for Modeling and Computational Reduction*, ser. Modeling, Simulation and Applications, A. Quarteroni and G. Rozza, Eds. Cham: Springer, 2014, pp. 159–185.

[8] R. D. Slone, R. Lee, and J.-F. Lee, "Well-conditioned asymptotic waveform evaluation for finite elements," *IEEE Transactions on Antennas and Propagation*, vol. 51, no. 9, pp. 2442–2447, 2003.

[9] R. D. Slone, R. Lee, and J.-F. Lee, "Broadband model order reduction of polynomial matrix equations using single-point well-conditioned asymptotic waveform evaluation: derivations and theory," *International Journal for Numerical Methods in Engineering*, vol. 58, no. 15, pp. 2325–2342, 2003.

[10] M. S. Lenzi, S. Lefteriu, H. Beriot, and W. Desmet, "A fast frequency sweep approach using padé approximations for solving helmholtz finite element models," *Journal of Sound and Vibration*, vol. 332, no. 8, pp. 1897–1917, 2013.

[11] R. Rumpler and P. Göransson, "An assessment of two popular padé-based approaches for fast frequency sweeps of time-harmonic finite element problems," *Proceedings of Meetings on Acoustics*, vol. 30, no. 1, p. 022003, 2017.

[12] G. A. Baker Jr. and P. Graves-Morris, *Pade Approximants*. Cambridge University Press, Nov. 2007.

[13] P. Avery, C. Farhat, and G. Reese, "Fast frequency sweep computations using a multi-point padé-based reconstruction method and an efficient iterative solver," *International Journal for Numerical Methods in Engineering*, vol. 69, no. 13, pp. 2848–2875, 2007.

[14] P. Guillaume, "Nested multivariate padé approximants," *Journal of Computational and Applied Mathematics*, vol. 82, no. 1-2, pp. 149–158, sep 1997.

[15] R. Rumpler, P. Göransson, and H. J. Rice, "An adaptive strategy for the bivariate solution of finite element problems using multivariate nested padé approximants," *International Journal for Numerical Methods in Engineering*, vol. 100, no. 9, pp. 689–710, sep 2014.

[16] C. Beattie and S. Gugercin, "Interpolatory projection methods for structure-preserving model reduction," *Systems & Control Letters*, vol. 58, no. 3, pp. 225–232, 2009.

[17] M. Czarniewska, G. Fotyga, A. Lamecki, and M. Mrozowski, "Parametrized local reduced-order models with compressed projection basis for fast parameter-dependent finite-element analysis," *IEEE Transactions on Microwave Theory and Techniques*, vol. 66, no. 8, pp. 3656–3667, 2018.

[18] D. Panagiotopoulos, E. Deckers, and W. Desmet, "Krylov subspaces recycling based model order reduction for acoustic bem systems and an error estimator," *Computer Methods in Applied Mechanics and Engineering*, vol. 359, p. 112755, 2020.

[19] V. De La Rubia, U. Razafison, and Y. Maday, "Reliable fast frequency sweep for microwave devices via the reduced-basis method," *IEEE Transactions on Microwave Theory and Techniques*, vol. 57, no. 12, pp. 2923–2937, 2009.

[20] U. Hetmaniuk, R. Tezaur, and C. Farhat, "An adaptive scheme for a class of interpolatory model reduction methods for frequency response problems," *International Journal for Numerical Methods in Engineering*, vol. 93, no. 10, pp. 1109–1124, 2013.

[21] R. Rumpler, P. Göransson, and J.-F. Deü, "A finite element approach combining a reduced-order system, Padé approximants, and an adaptive frequency windowing for fast multi-frequency solution of poro-acoustic problems," *International Journal for Numerical Methods in Engineering*, vol. 97, no. 10, pp. 759–784, 2014.

[22] M. Rewieński, A. Lame, M. Mrozowski *et al.*, "A goal-oriented error estimator for reduced basis method modeling of microwave devices," *IEEE Microwave and Wireless Components Letters*, vol. 25, no. 4, pp. 208–210, 2015.

[23] E. Creixell-Mediante, J. S. Jensen, F. Naets, J. Brunskog, and M. Larsen, "Adaptive parametric model order reduction technique for optimization of vibro-acoustic models: Application to hearing aid design," *Journal of Sound and Vibration*, vol. 424, pp. 208–223, 2018.

[24] L. Feng, A. C. Antoulas, and P. Benner, "Some a posteriori error bounds for reduced-order modelling of (non-) parametrized linear systems," *ESAIM: Mathematical Modelling and Numerical Analysis*, vol. 51, no. 6, pp. 2127–2158, 2017.

[25] L. Feng and P. Benner, "A new error estimator for reduced-order modeling of linear parametric systems," *IEEE Transactions on Microwave Theory and Techniques*, vol. 67, no. 12, pp. 4848–4859, 2019.

[26] R. Rumpler, "Padé approximants and the modal connection: Towards increased robustness for fast parametric sweeps," *International Journal for Numerical Methods in Engineering*, vol. 113, no. 1, pp. 65–81, 2018.

[27] M. Delany and E. Bazley, "Acoustical properties of fibrous absorbent materials," *Applied Acoustics*, vol. 3, no. 2, pp. 105–116, 1970.

[28] Y. Miki, "Acoustical properties of porous materials: Modifications of delany-bazley models," *Journal of the Acoustical Society of Japan (E)*, vol. 11, no. 1, pp. 19–24, 1990.